Supplement of E&G Quaternary Sci. J., 73, 1–22, 2024
https://doi.org/10.5194/egqsj-73-1-2024-supplement

Open Access E&G Quaternary Science Journal

Supplement of

Reconstructing the Eemian to Middle Pleniglacial pedosedimentary evolution of the Baix loess–palaeosol sequence (Rhône Rift Valley, southern France) – basic chronostratigraphic framework and palaeosol characterisation

Nora Pfaffner et al.

Correspondence to: Nora Pfaffner (nora.pfaffner@protonmail.com)

Methods – Luminescence screening

The luminescence screening aimed at a vertical sequence of roughly assessed OSL age estimates for the lower ca 7 m of the loess palaeosol sequence at the Baix section. The profiling encompassed two analytical steps: (1) rough assessment of the palaeodose of minimally prepared samples by applying the single aliquot regeneration (SAR) protocol (Murray and Wintle, 2000), and (2) determination of radionuclide concentrations for dose-rate assessment on a limited number of representative samples. While preparatory steps and palaeodose assessment were performed in the Heidelberg luminescence laboratory under strongly subdued indirect red light, radionuclide determination was performed in the Giessen luminescence laboratory. As the here applied luminescence screening provides only rough OSL age estimates, "age estimates" will be placed in quotation marks.

S1 A sequence of 1-cm³ subsamples

First, the sediment-soil blocks sampled in the flower boxes (hereinafter box samples) in the field were sub-sampled to obtain material not affected by daylight. We extracted small subsamples (1 cm x 1 cm x 1 cm) with a square frame for cutting out cubes (similar to those used for collecting 1 cm³-subsamples for pollen analyses from lake-sediment cores). We sampled along a vertical centre line of the sediment block at intervals of 5 cm (midpoint to midpoint; base area 1 cm x 1 cm; 4 cm distance from sample rim to sample rim), leaving 3.5 cm (midpoint 4 cm) distance from the possibly light-influenced rims at the top and bottom. We retrieved 8 subsamples (A–H) from each block (6 subsamples A–F from the lowermost box block, 1325–1357/1362 cm depth); in total 126 subsamples. The subsamples were weighed, dried at 50 °C and weighed again to determine the water content. We reserved material of some representative subsamples for radionuclide determination (cf. sect. S7).
Beneath each dose-rate sample, a second 1 cm³-cube sample was collected for luminescence analyses. Between the sampling of the first (upper, dose-rate sample) and the second 1 cm³-cube (lower, luminescence sample), the surface of the sediment-soil block was cleaned using a vacuum cleaner to prevent contamination with possibly light-influenced material from near the block-surface.

S2 Preparation of polymineral coarse grains and aliquot preparation

The 1 cm³-luminescence samples were minimally prepared, omitting, e.g. the destruction of organic matter and carbonates. The preparation included: wet sieving (125 µm) with dest. H_2O retaining the coarse-grain fraction ≥125 µm. This fraction was dried and used for preparing small aliquots (a few 10^2 grains) of polymineral coarse grains, strewn on aluminium cups (ø ca 10 mm, 1 mm thick) through a hole mask (ø 4 mm) and fixed with silicon oil. The theoretical maximum grain size fitting in the pit of the "spoon" used for aliquot preparation is ca 1 mm. However, such large grain sizes were not part of the coarse-grain aliquots as (1) we did not prepare single-grain aliquots; (2) the smaller grains accumulating in the bottom pit of the sample tube were deliberately spooned out, and (3) larger grains were shaken off the sample carrier. Therefore, grains are ≤500 µm in diameter. Microscopic inspection of aliquots after the OSL measurements confirmed this assumption but revealed that the aliquots might have included particles <125 µm. We assume that due to the omission of sample treatment with acetic acid and hydrogen peroxide and due to using soft-screen fabric instead of metal sieves for the rapid preparation soil aggregates were not disaggregated completely prior to/during the sieving but only later when spooned out of the

sample container for aliquot preparation. Yet it is reasonable to assume that the dominant OSL signal originates from the coarse-grain fraction.

S3 Measurement equipment for equivalent dose (D_e) determination

SAR measurements for equivalent dose (D_e) determination were performed on two luminescence readers, i.e. a Risø reader model TL/OSL DA20 (serial number 240, nicknamed "Athenaeum") and a Risø reader model TL/OSL DA15, updated DA20 (serial number 83) (cf. Lapp et al., 2012, 2015). Both readers were equipped with a turntable with 48 sample positions, three clusters of infrared emitting diodes (7 LEDs each; 870 Δ 40 nm; plus longpass filter RG830 (Schott) for No. 83) for infrared stimulated luminescence (IRSL), four clusters of blue light-emitting diodes (7 LEDs each; 470 Δ 30 nm) for blue light stimulated luminescence (BLSL), a bialkali PMT EMI 9235QB15 for signal detection, a $^{90}Sr/^{90}Y$ β-source (No. 240: ca 5.0 Gy min^{-1} at the time of measurements 2020–2021; No. 83: ca 3.6 Gy min^{-1}) for laboratory irradiation. The system was run with Risø MiniSys software version 4.08 (12.01.2016). Measurements were run with the Risø sequence editor v4.36 (2015-09-10). OSL measurements were performed in an N_2 atmosphere after an atmosphere stabilisation period of ca 4 min at the beginning of a SAR measurement.

S4 Adapting the single-aliquot regeneration (SAR) protocols

For the luminescence screening, palaeodose determination on the polymineral coarse grains was performed in a twofold manner, once with a blue-light stimulated luminescence (BLSL) SAR protocol (Murray and Wintle, 2000), including IR-bleaching prior to the BLSL readout (pIR-BLSL), and once with a post-infrared (at 60 °C) infrared (at 225 °C) stimulation ($pIR_{60}IR_{225}$) protocol (Thomsen et al., 2008). For the BLSL measurements, 3 aliquots were analysed from each of the 126 subsamples (HDS-1802 A to HDS-1817 F). For the $pIR_{60}IR_{225}$ protocol, we limited the measurements to one aliquot per subsample, as the latter measurements lasted significantly longer.

The uppermost (HDS-1802) and the lowermost sample (HDS-1817) were used to adapt the measurement parameters of the SAR protocols. For data analysis and for D_e determination, we used the software "Analyst" (Duller, 2015 Version 4.31.9, Build 23rd May 2020; for details of the data analysis, cf. Table S1 and Table S2).

Examples of pIR-BLSL and $pIR_{60}IR_{225}$ shine-down, as well as dose-response curves, are provided in sections S4.1.2 (Fig. S1), S4.1.3 (Fig. S3) and S4.2.3 (Figs. S5, S6).

S4.1 pIR-BLSL SAR protocol

For the pIR-BLSL SAR protocol, signal detection occurred in the ultra-violet spectrum around 340 nm through a set of glass filters U340 (Schott; 3 x 2.5 mm each) on luminescence reader No. 83. The IR- and BL-stimulation power was set to 90 %.

IR-stimulation at 125 °C which was performed to deplete a potential signal of feldspar, thus "enriching" the signal of quartz from the polymineral coarse-grains (cf. also Banerjee et al., 2001), and BL-stimulation at 125 °C were each performed for 40 s (250 data channels; 0.16 s per data channel) (cf. Table S1). Dose-response curves were fitted with a single exponential function. The D_e integral was set to (0–0.16 s) and the background integral to 32.16–40.0 s. The SAR protocol as adapted in a series of pre-tests (sect. S4.1.1 to S4.1.3) is shown in Fig. 4 of the main text.

Table S1: Parameters of data analysis for D_e determination – pIR-BLSL SAR protocol.

Software:	Luminescence Analyst, version 4.31.9 (Duller 2015)
Curve fitting:	Exponential fit
Integral [channel]:	1 - 1 (0 - 0.16 s)
Background [channel]:	201 - 250 (32.16 - 40.0 s)
Use recycled points for fitting:	Yes
Measurement error [%]	1.5
Incorporate error on curve fitting:	Yes
Use errors when applying criteria:	Yes
Recycling ratio limit [%]:	10
Maximum test dose error [%]:	10
Maximum recuperation [% of N]:	10
Tn signal > 3 sigma above background:	Yes

S4.1.1 D_e-range test

The potential range of D_es was investigated on unprocessed sediment material crumbled on aluminium cups (ø ca 10 mm) and fixed with silicon oil. This was done with a pIR-BLSL SAR protocol using preheat 1 of 200 °C and preheat 2 of 160 °C and seven regeneration dose points (560 s, 980 s, 1400 s, 1820 s, 2240 s, 0 s, 1400 s) spanning the range ca 33.5–109 Gy and a normalisation dose (test dose) of 830 s (49.7 Gy). The dose-response curve conforms to an expected dose of ca 84 Gy representing 100 %, with regeneration dose points at 40 %, 70 %, 100 %, 130 %, 160 %, 0 % (testing signal recuperation) and 100 % (recycling dose point) of the expected dose. The range test was applied on 42 aliquots from the uppermost box sample (HDS-1802, subsamples A–H) and the lowermost box sample (HDS-1817, subsamples A–F), 3 aliquots per subsample. D_e determination occurred on the first data channel (0–0.16 s), with the last 50 data channels (32.16–40 s) used for late light subtraction. Criteria of acceptance were a 10 % recycling ratio, a maximum test dose error of 10 % and a maximum recuperation of 10 %. For this initial test, also D_es that had to be extrapolated beyond the largest regeneration dose point were accepted. The obtained D_es varied between 72–193 Gy (results not shown).

As fine grain material may coat coarser grains and aggregate as soil peds, for further measurements, the fraction <125 µm was eliminated by wet sieving, and the strategy changed from no sample preparation to minimal sample preparation (cf. sect. S2).

Further tests (not shown here) investigated whether the normalisation dose could be reduced to 350 s (ca 21 Gy), corresponding to 60 % to 25 % of the expected dose. As these tests proved positive, the lower normalisation dose was applied in further tests.

S4.1.2 Dose recovery uppermost sample (HDS-1802 A–H)

A dose-recovery test was performed on eight aliquots of the uppermost box sample HDS-1802, subsamples A–H, one aliquot each, bleached under the solar simulator for 3 h prior to irradiation. The administered laboratory dose was 1400 s (ca 84 Gy), and – like in the previous tests – the positions of the seven regeneration dose points were at 40 %, 70 %, 100 %, 130 %, 160 %, and 0 % of the laboratory dose (cf. Fig. S1) and the normalisation dose was 350 s (25 %) (henceforth the 1400 s growth curve). As a result, most aliquots met the expected D_e within error margins, and all aliquots were within a tolerance of 10 %. The expected dose was met within error margins by the mean (1345.3 ± 75.6 s), but the centre values (mean, central dose) underestimated the given dose slightly by 4–5 % (Fig. S2).

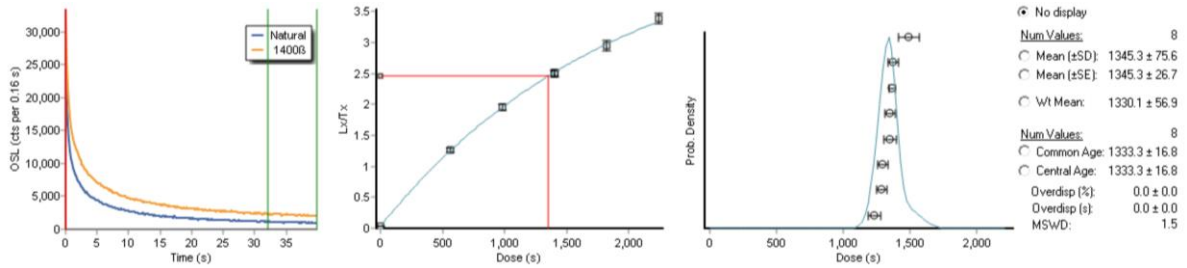

Figure S1: Dose recovery test on eight aliquots of box sample HDS-1802, subsamples A–H, one aliquot each. Example of shine down curves (left), SAR dose response curve (center) and probability density plot of recovered doses. The laboratory dose of ca 84 Gy (1400 s) was recovered within a tolerance of 10 %. Graphical output from "Analyst" (Duller, 2015).

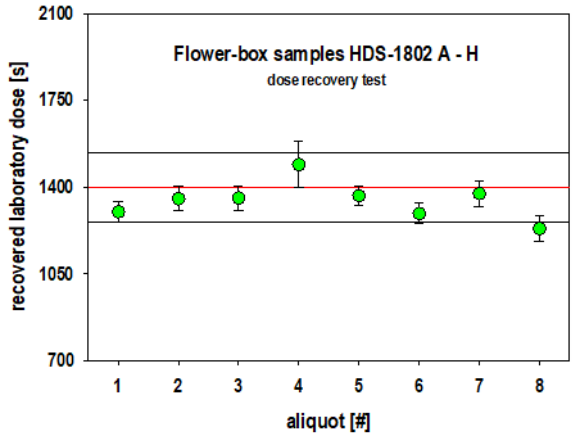

Figure S2: pIR-BLSL dose recovery test on eight aliquots of box sample HDS-1802, subsamples A–H, one aliquot each. The laboratory dose of ca 84 Gy (1400 s) was recovered within a tolerance of 10 %.

S4.1.3 Dose recovery tests lowermost sample (HDS-1817 A–F)

Another dose recovery test was performed on twelve aliquots of the lowermost box sample HDS-1817, subsamples A–F, two aliquots each. The laboratory dose was set to ca 191 Gy, and the seven regeneration dose points at 40 %, 60 %, 100 %, 130 %, 160 %, 0 % and 100 % of the expected dose were adjusted accordingly (1280 s, 2240 s, 3200 s, 4160 s, 5120 s, 0 s and 3200 s) (henceforth the 3200 s growth curve) (cf. Fig. S3). As for the dose recovery test with the 1400 s growth curve on sample HDS-1802, the normalisation dose was 350 s (for deposited doses in Gy cf. Fig. 4 of the main text). As a result, the centre value of the mean and central dose underestimated the expected dose slightly by ca 5 %. All recovered D_es were recovered within 10 % of the expected dose (Fig. S4).

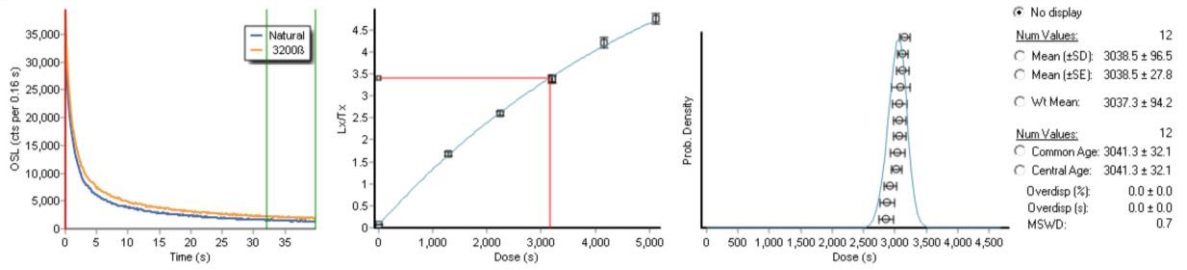

Figure S3: Dose recovery test on twelve aliquots of box sample HDS-1817 subsamples A–F, two aliquots each. Example of shine down curves (left), SAR dose-response curve (centre) and probability density plot of recovered doses. The laboratory dose of ca 191 Gy (3200 s) was recovered within a tolerance of 10 %. Graphical output from "Analyst" (Duller, 2015).

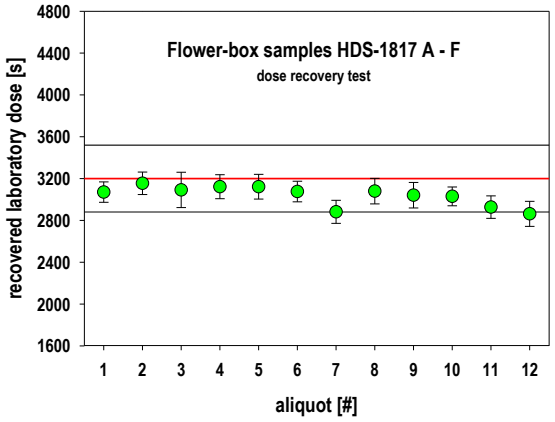

Figure S4: pIR-BLSL dose recovery test on twelve aliquots of box sample HDS-1817, subsamples A–F, two aliquots each. The laboratory dose of ca 191 Gy (3200 s) was recovered within a tolerance of 10 %.

We considered the results of both dose-recovery tests acceptable for the intended OSL screening. Therefore, the pIR-BLSL protocol was used for the "dating" measurements applying the 1400 s dose-response curve for samples HDS-1802 to HDS-1808 and the 3200 s dose-response curve for samples HDS-1809 to HDS-1817 (cf. Fig. 4 of the main text).

S4.2 $pIR_{60}IR_{225}$ measurements

The $pIR_{60}IR_{225}$ signal was detected in the blue-violet spectrum around 410 nm through an interference filter CH-30D410-44.3 (Chroma) on the luminescence reader "Athenaeum". Only every second turntable position was used for SAR measurements to minimise unwanted optical cross-talk during IR stimulation (Kreutzer et al., 2013). The stimulation power was set to 90 %. IR-stimulation at 60 °C and subsequently at 225 °C was performed for 200 s (1 s per data channel) (cf. Table S2). For the data analysis, the first four seconds were used as D_e integral, while the integral 51–60 s was used for background subtraction (testing also other D_e-integral and background combinations, which all provided same results within error margins; cf. Tables S3–S5). The pIR-IR SAR protocol, as adapted in a series of pre-tests (sect. S4.2.1 to S4.2.3) is shown in Fig. 5 of the main text.

Table S2: Parameters of data analysis for D_e determination – $pIR_{60}IR_{225}$ SAR protocol.

Software:	Luminescence Analyst, version 4.31.9 (Duller 2015)
Curve fitting:	Exponential fit
Integral [channel]:	1 - 4 (0 - 4 s)
Background [channel]:	51 - 60 (51 - 60 s)
Use recycled points for fitting:	Yes
Measurement error [%]:	1.5
Incorportae error on curve fitting:	Yes
Use errors when applying criteria:	Yes
Recycling ratio limit [%]:	10
Maximum test dose error [%]:	10
Maximum recuperation [% of N]:	10
Tn signal > 3 sigma above background:	Yes

S4.2.1 D_e-range test

A $pIR_{60}IR_{225}$-SAR-protocol was applied to 14 aliquots of the uppermost sample HDS-1802 (8 subsamples, A–H, one aliquot each) and the lowermost sample HDS-1817 (6 subsamples, A–F, one aliquot each) to get an idea of the possible D_e range of the box samples. The preliminary dose-response curve was constructed with regeneration

dose points at ca 33.1 Gy, 57.8 Gy, 82.6 Gy, 107.4 Gy, 132.2 Gy, 0 Gy and 82.6 Gy. The normalisation dose (test dose) was set to 600 s (ca 49.6 Gy, or 60 % of the 100 % regeneration dose point). The measurement started after 4 min (120 s + 120 s) N-purge. IR-stimulation at 60 °C and subsequently at 225 °C was performed for 200 s (1 s per data channel). The first four seconds were used as D_e integral for the data analysis. The integral 51–60 s was used for background subtraction. For $IR_{225,}$ three aliquots were not analysable, as the potential D_e value was too large to be met by the (extrapolated) SAR dose-response curve, the $D_e s$ of the remaining 11 aliquots had to be extrapolated beyond the largest regeneration dose point. $D_e s$ scattered between ca 2000 s to 8200 s (ca 165–678 Gy) (results not shown).

S4.2.2 Normalisation dose test

IR SAR and pIR-IR SAR measurements respond sensitively to the size of the normalisation dose (unpublished data in the Heidelberg luminescence laboratory; Colarossi et al., 2018). Therefore, eight aliquots of HDS-1802 A–H (one aliquot each) were subjected to a combined dose-recovery and normalisation dose test. Based on the D_e range test (cf. sect. S4.2.1) and keeping the spreading of the regeneration dose points at 40 %, 70 %, 100 %, 130 %, 160 %, 0 % and 100 % of the expected dose, the regeneration dose points were set at 1560 s, 2730 s, 3900 s, 5070 s, 6240 s, 0 s and 3900 s with 3900 s corresponding to 321.3 Gy and 6240 s corresponding to 514.2 Gy (3900 s dose-response curve). We tested which size of the normalisation dose would be appropriate for the given dose-response curve, testing 98 s, 195 s, 293 s, 390 s, 780 s, 1170 s, 1560 s, 1950 s, corresponding to 2.5 %, 5 %, 7.5 %, 10 %, 20 %, 30 %, 40 % and 50 % of the expected dose. Using again the integral 51–60 s for late light subtraction, the D_e determination shows within error margins the same results for different lengths of the D_e integral varying from one to four seconds (Table S3). Whereas the smallest two normalisation doses of 2.5 % and 5 % of the expected dose appear to overestimate the given dose (more strongly curved dose-response curve), the largest five normalisation doses seem to underestimate the laboratory dose slightly. Therefore, we chose **293 s** (ca 24.1 Gy; 7.5 % of the expected dose) as normalisation for further tests and measurements.

Table S3: Results of the normalisation dose test for late light subtraction 51–60 s and four different D_e integrals.

normalisation dose	0 - 1 s		0 - 2 s		0 - 3 s		0 - 4 s	
[% of expected dose]	DE [s]		DE [s]		DE [s]		DE [s]	
2.5	4321.87	± 311.31	4308.89	± 292.71	4338.25	± 288.70	4328.72	± 294.48
5	4431.09	± 270.47	N.A.		4408.31	± 249.13	4425.11	± 247.50
7.5	3975.52	± 164.97	3992.28	± 163.79	3991.09	± 162.31	3993.61	± 161.83
10	3684.01	± 194.39	3730.01	± 177.66	3705.55	± 170.96	3696.81	± 172.75
20	3775.38	± 137.88	3799.88	± 132.67	3782.96	± 127.59	3749.76	± 125.23
30	3864.34	± 139.05	3852.31	± 128.61	3855.32	± 127.51	3860.00	± 127.49
40	3296.93	± 135.32	3365.37	± 131.58	3315.31	± 127.13	3315.33	± 126.48
50	3841.49	± 136.91	3813.95	± 128.56	3815.51	± 129.27	3795.68	± 126.49

S4.2.3 Dose-recovery tests (HDS-1802 A–H)

A dose-recovery test with an administered dose of 3900 s and a normalisation dose of 293 s was performed on the eight previously measured aliquots of HDS-1802 A–H (one aliquot each). D_e analysis occurred with a late light subtraction of the integral 51–60 s. As a result, the expected dose is recovered well (cf. Fig. S5, Table S4). The mean recuperation is 4.9 % for the D_e integral 0–4 s and 4.8 % for the integral 0–1 s.

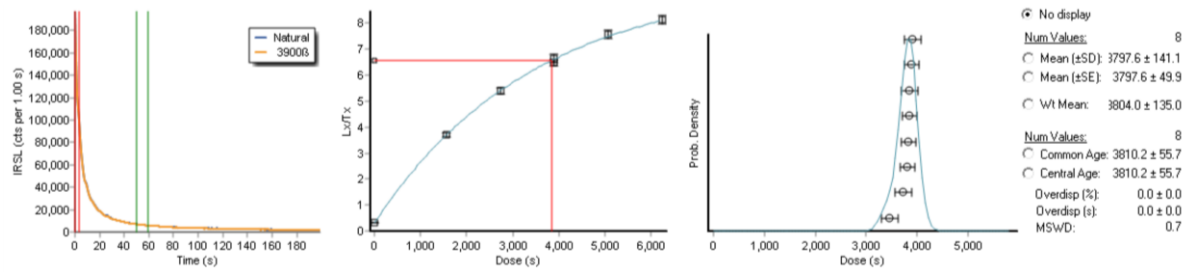

***De* integral 0–4 s**

Figure S5: Dose recovery test on the eight aliquots already used in the previous normalisation dose test with a normalisation dose of 293 s (7.5 % of expected dose). Graphical output from "Analyst" (Duller, 2015).

Table S4: Dose recovery test on the eight aliquots already used in the previous normalisation dose test with a normalisation dose of 293 s (7.5 % of expected dose).

aliquot	0 - 1 s		0 - 2 s		0 - 3 s		0 - 4 s	
[turntable position]	DE [s]		DE [s]		DE [s]		DE [s]	
1	3900.96	± 172.35	3858.07	± 163.51	3862.69	± 163.67	3849.25	± 162.86
3	3816.54	± 156.18	3811.22	± 152.53	3846.35	± 154.64	3846.49	± 153.94
5	3881.11	± 146.21	3886.13	± 142.19	3901.84	± 142.58	3899.61	± 142.97
7	3790.21	± 217.63	3860.51	± 192.39	3761.31	± 177.68	3741.60	± 169.23
9	3825.75	± 167.62	3792.26	± 152.46	3816.67	± 151.13	3823.42	± 149.78
11	3988.69	± 170.88	3942.14	± 158.66	3840.26	± 150.13	3836.75	± 149.18
13	3785.95	± 211.60	3582.07	± 177.33	3489.28	± 166.45	3472.45	± 166.63
15	3992.57	± 205.95	3852.80	± 176.19	3880.96	± 171.56	3911.10	± 172.09

In a further dose-recovery test with a given dose of 3900 s and a normalisation dose of 239 s, eight aliquots of HDS-1802 A–H (one aliquot each) were analysed, which had been bleached for 3 h under the solar simulator (Fig. S6). The results show that the expected dose was overestimated by ca 8 % (here: D_e integral 0–1 s, late light 51–60 s; mean with standard deviation and standard error 4225.3 ± 148.8 ± 52.6 s; central dose 4220.4 ± 75.8 s). Yet all recovered D_e values were reproduced within a range of 10 % of the expected value (Fig. S7). No dependency was observed on the D_e integral and/or the integral used for late light subtraction (Table S5). Like the dose recovery test on the previously measured aliquots, the mean recuperation was ca 5 % (here D_e integral 0–4 s, late light subtraction 51–60 s).

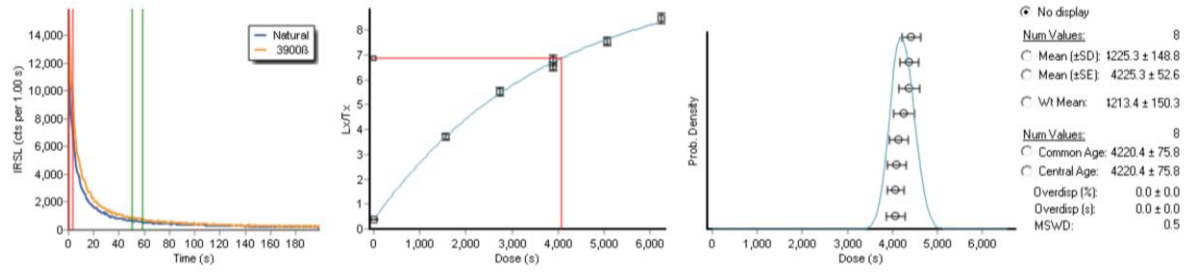

***De* integral 0–4 s, late light integral 51–60 s**

Figure S6: Results of the dose recovery test on eight fresh aliquots bleached under the solar simulator with a normalisation dose of 293 s (7.5 % of expected dose). Graphical output from "Analyst" (Duller, 2015).

Table S5: Results of the dose recovery test on eight fresh aliquots bleached under the solar simulator with a normalisation dose of 293 s (7.5 % of expected dose).

late light	51 - 60 s		51 - 60 s		51 - 60 s		51 - 60 s		5 - 6 s	
aliquot	0 - 1 s		0 - 2 s		0 - 3 s		0 - 4 s		0 - 1 s	
[turntable position]	De [s]		De [s]		De [s]		De [s]		De [s]	
1	4555.36	± 264.61	4289.56	± 216.80	4335.93	± 212.05	4379.03	± 207.60	4684.07	± 383.98
3	4399.35	± 226.94	4429.46	± 222.55	4441.49	± 225.83	4415.74	± 223.90	4409.43	± 249.60
5	4085.18	± 268.00	3935.28	± 225.06	4025.33	± 215.23	4066.29	± 214.89	4198.90	± 450.01
7	4424.18	± 298.52	4395.39	± 254.14	4259.88	± 226.22	4372.11	± 231.07	5150.97	± 613.59
9	4205.14	± 259.28	4090.86	± 222.31	4043.40	± 212.95	4091.24	± 215.13	4214.32	± 346.01
11	4614.07	± 366.87	4461.79	± 304.13	4354.10	± 267.77	4256.15	± 245.28	4434.31	± 527.35
13	3963.13	± 202.50	3989.48	± 184.38	4077.71	± 185.10	4071.44	± 180.86	3930.60	± 261.32
15	4167.14	± 266.13	4192.96	± 229.95	4165.17	± 219.48	4150.44	± 211.97	4064.28	± 368.20

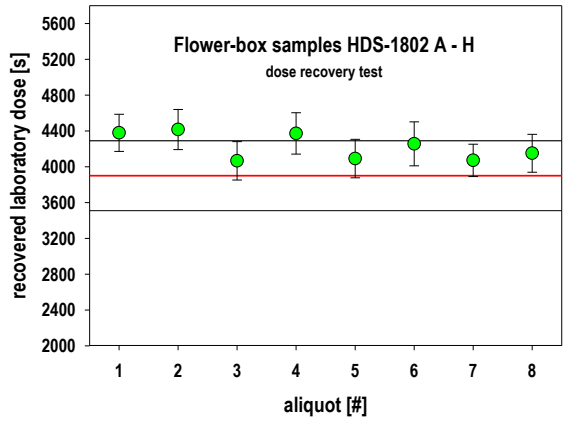

Figure S7: $pIR_{60}IR_{225}$ dose recovery test on eight aliquots of box sample HDS-1802, subsamples A–H, one aliquot each. The laboratory dose of ca 321.3 Gy (3900 s) was recovered within a tolerance of 10 %.

As the results appeared acceptable for the intended OSL screening (rather than proper OSL dating) and as sample material was scarce, no further tests potentially improving the $pIR_{60}IR_{225}$ SAR protocol were performed. We used one dose-response curve suitable for interpolating all, or at least most, of the expected palaeodoses. Due to the measurement time, only one aliquot per subsample was analysed. Figure 5 of the main text gives a schematic overview of the $pIR_{60}IR_{225}$ SAR protocol applied for the palaeodose assessments.

S5 Testing for anomalous signal fading

In luminescence dating, feldspar is known for a phenomenon termed athermal signal fading (Wintle, 1973), i.e. an unwanted signal loss. Therefore, fading tests are usually associated with luminescence dating measurements of feldspar (e.g. Auclair et al., 2003). Here we tested the 8 aliquots of the 8 subsamples of sample HDS-1803 and the 6 aliquots of the 6 subsamples of sample HDS-1817 for the $pIR_{60}IR_{225}$ protocol. The signal readout was performed two times promptly, after ca 1 day, 2 days, 4 days, and promptly again.

As IR-bleaching in the pIR-BLSL protocol reduces the signal detected from feldspar but does not exclude signal from feldspar during the subsequent BLSL step completely, few aliquots measured with the pIR-BLSL aliquot were also subjected to a fading test: the 6 aliquots of subsamples F and G of sample HDS-1802 as well as 6 aliquots of sample HDS-1817, subsamples A and C (2 aliquots each), and B and D (1 aliquot each). A signal readout on HDS-1802 was two times prompt, after ca 4 h, 1 day, 2 days and prompt again; on HDS-1817, readout occurred two times prompt, after ca 1 day, 2 days, 4 days, and prompt.

Data analysis and *g*-value determination were performed with the function analyse_FadingMeasurements (Kreutzer and Burow, 2000) from the R package 'Luminescence' (Kreutzer et al., 2012). Results of the fading measurements are provided in supplement 2 Results – Luminescence screening).

S6 Converting beta-irradiation time to deposited energy

Beta irradiation must be converted to deposited energy in the analysed mineral grains, which is accomplished using a calibrated beta source. The amount of deposited energy per unit time is known (e.g. Gy per min or s irradiation time). The luminescence readers used in this study had been calibrated using a grain-size fraction of 90–125 µm (corresponding to a grain-size fraction ca 130–165 µm before HF-etching). However, the ca 1 cm³ samples were too small for rigorous sieving for technical reasons. Therefore, only the lower boundary of the grain-size fraction was well defined (cf. sect. S2), while the upper boundary was estimated at 500 µm at maximum. However, the amount of energy deposited in mineral grains by beta irradiation in luminescence readers does not change significantly for grain size diameters varying in the range ca 100–500 µm (Armitage and Bailey, 2005; Mauz et al., 2021). Potential errors in the beta-source calibration of few percentages due to slightly differing grain sizes in the here analysed grain-size spectrum is a minor issue when compared to other challenges associated with gamma to beta transfer calibration (Kadereit and Kreutzer, 2013; Tribolo et al., 2019; Richter et al., 2020).

S7 Dose rate determination

From the 1 cm³-cubes used for water-content determination, six samples were selected for radionuclide determination (Table S6). The samples originate from: (1) the top of the sampled sediment-soil column (BCk3; 575/590–700 cm); (2) the upper interstadial soil (5 Bw2: 745–775 cm); (3) the loess deposit beneath (5 Ck2: 915–995 cm); (4) the lower interstadial soil (6 Bw3: 1080–1155 cm); (5, 6) and the possibly reworked palaeosol remains of the interglacial soil-complex (7 Btg: 1227–1275 cm; 7 Bt1: 1315–1360 cm). The selected subsamples were regarded as adequate for deriving a "representative" mean dose rate to be used for OSL "age estimate" assessments.

Table S6: Six subsamples (>3 g dry wt.) of the box samples HDS-1802 to HDS-1817 were selected for dose-rate determination with the *µ*Dose system.

Flower-Box [Lab.-code]	Subsample [A - H]	Depth b.g.l. [cm]	Weight dry mass [g]	Soil horizon [after FAO 2014/2015]	Comment
HDS-1802	C	672.5	3.95	(11) 575/590 - 700 cm ***3 BCk3***	representing "everything" above MIS 3 soil
HDS-1803					
HDS-1804	B	764.5	5.80	(13) 745 - 775 cm: ***5 Bw2***	MIS 3 soil (?)
HDS-1805					
HDS-1806					
HDS-1807					
HDS-1808	E	963.5	4.15	(18) 915 - 995 cm: ***5 Ck2***	with brown sediment infillings in former root channels
HDS-1809					
HDS-1810					
HDS-1811	F	1091.5	5.65	(20) 1080 - 1120 cm: ***6 Bw3***	with soft Mn concretions
HDS-1812					
HDS-1813					
HDS-1814					
HDS-1815	E	1256.5	4.85	(26) 1227 - 1275 cm: ***7 Btg***	hydromorphic features and bleached root channels
HDS-1816					
HDS-1817	E	1349.5	3.65	(28) 1315 - 1360 cm: ***8 Bt1***	reworked Eem Bt (?)

As the samples were relatively small, weighing ca 2.05–6.95 g each (dry wt.), the recently developed *µ*Dose-system (Tudyka et al., 2018, 2020) was regarded as especially suitable for dose-rate determination within the here performed luminescence screening at the Baix site. The selection of representative samples from different B and C horizons occurred among those that had provided at least 3 g of dry matter. A comprehensive performance test of the novel device for dose-rate determination has recently been conducted by Kolb et al. (2022), which showed that the *µ*Dose-analytics delivers mostly equally correct results as established techniques such as, e.g. low-level

gamma-ray spectrometry. μDose measurements were performed in the Giessen luminescence laboratory, where the samples were dried at 105 °C before 3 g of each sample were placed and sealed in the μDose sample holders.

S8 Age estimate calculations

OSL scanning "age estimates" were calculated not for mean burial doses of a set of aliquots but for individual aliquots. In contrast, a mean value was assumed for the dose rate based on the six representative dose rate samples. Assuming radioactive equilibrium, radionuclide concentrations were transformed to dose rate values by applying the dose-rate conversion factors of Guérin et al. (2011). The cosmic dose rate was calculated with the R package 'Luminescence' (Kreutzer et al., 2012) but contributed only between 0.1044 ± 0.0104 Gy ka^{-1} (uppermost sample at 6.72 m depth) and 0.0586 ± 0.0059 Gy ka^{-1} (lowermost sample at 13.49 m depth). For the mineral grains responding to IR stimulation by emitting a luminescence signal around 410 nm (likely potassium feldspar), an internal potassium content of 12.5 ± 1.25 wt.-% was assumed. Considering the efficiency of the external alpha radiation (a-value) for the pIR-IR feldspar measurements at 225 °C an *a*-value of 0.1 ± 0.02 (cf. Kreutzer et al., 2014) and for the mineral grains responding to BL-stimulation after IR-depletion (assumed to originate dominantly from quartz) an a-value of 0.035 ± 0.02 (cf. Lai et al., 2008) was taken into account, assuming that alpha particles penetrate 20 µm into the coarse grains and adapting the fine-grain *a*-values accordingly.

The water contents of the samples as measured (cf. Fig. S8) were not considered to be representative of the dating period. Therefore, we estimated a uniform water content (ratio of wet sample wt. to dry wt.) of Δ 1.17 ± 0.05, based on the considerations of Sauer et al. (2016), who calculated realistic water contents for pore volume distributions typical of loess. As also Bosq et al., (2020) had followed this recommendation for OSL dating at the Collias site ca 100 km further to the south, the procedure allows comparing the OSL dating results for the two sites. Only for the lowermost sample, a silt loam, in addition to a water content of Δ 1.28 ± 0.05 was assumed, thus simulating stagnic conditions.

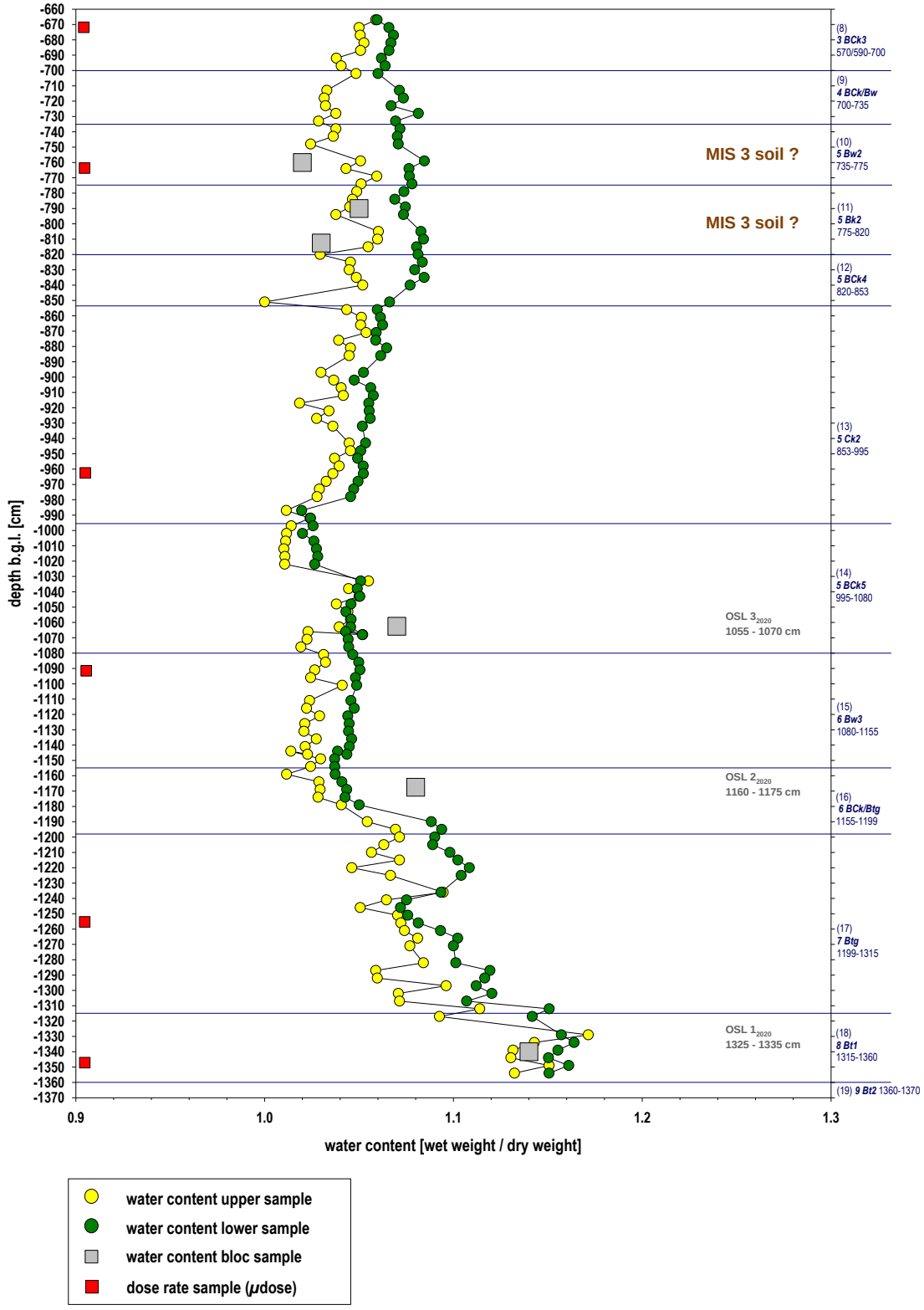

Figure S8: Results of the water content determination from the box subsamples. The lower samples (luminescence samples) are systematically slightly wetter than the upper samples (dose rate samples), likely due to water percolating in the downward direction into the horizontally stored sample blocks. Red squares denoting positions of dose rate samples used for *µ*Dose analyses. Grey squares illustrating water contents measured in additional block samples not further analysed in the present study. All data values within an error margin of ± 0.05. Smallest values above 1178 cm b.g.l. (6 BCk/Btg to top; mean ca 1.04 upper samples; ca 1.06 lower samples). Largest values in lowermost unit 8 Bt1 (1315–1360 cm b.g.l.; ca 1.14 upper samples; ca 1.16 lower samples). Intermediate resp. increasing values from 7 Btg to 6 BCk/Btg (ca 1.07 upper samples; ca 1.10 lower samples).

S9 Luminescence sensitivity

Varying luminescence count rates (sensitivities) within a loess profile may proxy different source areas or source material (Fitzsimmons et al., 2022). We measured both the IR- and the post-IR BL-stimulated luminescence of the minimally prepared box subsamples (cf. sect. S2.4.1). We used the ratio of both signals as a down-the-profile-normalised proxy, as the luminescence yield may also depend on the amount of material on a sample carrier rather than the mere luminescence sensitivity of a material. It is assumed that the IRSL signal indicates the presence of feldspar, while the BLSL signal points to quartz (e.g. Banerjee et al., 2001). However, as the IR stimulation does not fully erase the OSL signal in feldspar, the post-IR BLSL signal is likely a composite of quartz and feldspar. The comparatively mild preheat procedure of 10 s duration at 200 °C, suitable for quartz measurements, might further cause the preservation of a feldspar signal. Nevertheless, possible variations in the signal ratio likely indicate different provenance or weathering conditions (cf. Fitzsimmons et al., 2022).

The signal ratios were determined using the function `Luminescence::calc_OSLLxTxRatio()` of the R package 'Luminescence', version 0.9.16 (Kreutzer et al., 2021), pretending that the IR-induced signal was the L_x/L_n-signal and the post-IR BLSL-induced signal was the T_x/T_n signal (therefore larger ratios would point to more feldspar emitting around 340 nm, in the simplified model here taken as a basis). IRSL and BLSL signals were gained from the test-dose-induced luminescence. First, the 8 test-dose signals of a complete SAR measurement were averaged for each aliquot; then, the mean with standard error of the three aliquots measured of each subsample was calculated.

References

Armitage, S. J. and Bailey, R. M.: The measured dependence of laboratory beta dose rates on sample grain size, Radiat. Meas., 39, 123–127, https://doi.org/10.1016/j.radmeas.2004.06.008, 2005.

Auclair, M., Lamothe, M., and Huot, S.: Measurement of anomalous fading for feldspar IRSL using SAR, Radiat. Meas., 37, 487–492, https://doi.org/10.1016/S1350-4487(03)00018-0, 2003.

Banerjee, D., Murray, A., Bøtter-Jensen, L., and Lang, A.: Equivalent dose estimation using a single aliquot of polymineral fine grains, Radiat. Meas., 33, 73–94, https://doi.org/10.1016/S1350-4487(00)00101-3, 2001.

Bosq, M., Kreutzer, S., Bertran, P., Degeai, J.-P., Dugas, P., Kadereit, A., Lanos, P., Moine, O., Pfaffner, N., Queffelec, A., and Sauer, D.: Chronostratigraphy of two late Pleistocene loess-palaeosol sequences in the Rhône Valley (southeast France), Quat. Sci. Rev., 106473, https://doi.org/10.1016/j.quascirev.2020.106473, 2020.

Colarossi, D., Duller, G., and Roberts, H.M.: Exploring the behaviour of luminescence signals from feldspars: Implications for the single aliquot regenerative dose protocol, Radiat. Meas., 109, 35–44, https://doi.org/10.1016/j.radmeas.2017.07.005, 2018.

Duller, G.A.T.: The Analyst software package for luminescence data: overview and recent improvements, Ancient TL, 33, 35–42, http://ancienttl.org/ATL_33-1_2015/ATL_33-1_Duller_p35-42.pdf, 2015.

Fitzsimmons, K.E., Perić, Z., Nowatzki, M., Lindauer, S., Vinnepand, M., Prud'homme, C., Dave, A. K., Vött, A., and Fischer, P.: Luminescence Sensitivity of Rhine Valley Loess: Indicators of Source Variability?, Quaternary, 5, 1, https://doi.org/10.3390/quat5010001, 2022.

Guérin, G., Mercier, N., and Adamiec, G.: Dose-rate conversion factors: update, Ancient TL, 29, 5–8, https://www.aber.ac.uk/en/media/departmental/dges/ancienttl/pdf/vol29no1/atl-issue29-1.pdf#page=9, 2011.

Kolb, T., Tudyka, K., Kadereit, A., Lomax, J., Poręba, G., Zander, A., Zipf, L., and Fuchs, M.: The µDose system: determination of environmental dose rates by combined alpha and beta counting – performance tests and practical experiences, Geochronology, 4, 1–31, https://doi.org/10.5194/gchron-4-1-2022, 2022.

Kreutzer, S., Schmidt, C., Fuchs, M.C., Dietze, M., Fischer, M., and Fuchs, M.: Introducing an R package for luminescence dating analysis, Ancient TL, 30, 1–8, available at: https://hal.science/hal-01846159, 2012.

Kreutzer, S., Hülle, D., Jørkov Thomsen, K., Hilgers, A., Kadereit, A., and Fuchs, M.: Quantification of cross-bleaching during infrared (IR) light stimulation, Ancient TL, 31 (1), 1–10, http://www.ancienttl.org/ATL_31-1_2013/ATL_31-1_Kreutzer_p1-10.pdf, 2013.

Kreutzer, S., Schmidt, C., DeWitt, R., and Fuchs, M.: The a-value of polymineral fine grain samples measured with the post-IR IRSL protocol, Radiat. Meas., 69, 18–29, https://doi.org/10.1016/j.radmeas.2014.04.027, 2014.

Kreutzer, S. and Burow, C.: analyse_FadingMeasurement: Analyse fading measurements and returns the fading rate per decade (g-value). Function version 0.1.14. In: Kreutzer, S., Burow, C., Dietze, M., Fuchs, M.C., Schmidt, C., Fischer, M., Friedrich, J., 2020. Luminescence: Comprehensive Luminescence Dating Data Analysis. R package version 0.9.8.9000-17,

https://CRAN.R-projcet.org/package= Luminescence, 2020.

Kreutzer, S., Valladas, H., Texier, P.-J., Moineau, V., Mologni, C., and Mercier, N.: The Mousterian loess sequence La Combette (France) and its chronological framework: A re-investigation, Comptes Rendus Palevol., 20 (14), 225–525, https://doi.org/10.5852/cr-palevol2021v20a14, 2021.

Lai, Z., Zöller, L., Fuchs, M., and Brückner, H., Alpha efficiency determination for OSL of quartz extracted from Chinese loess, Radiat. Meas., 43, 767–770, https://doi:10.1016/j.radmeas.2008.01.022, 2008.

Lapp, T., Jain, M., Thomsen, K. J., Murray, A.S., and Buylaert, J.-P.: New luminescence measurement facilities in retrospective dosimetry, Radiat. Meas., 47, 803–808, https://doi.org/10.1016/j.radmeas.2012.02.006, 2012.

Lapp, T., Kook, M., Murray, A.S., Thomsen, K.J., Buylaert, J.-P., and Jain, M.: A new luminescence detection and stimulation head for the Risø TL/OSL reader, Radiat. Meas., 81, 178–184, https://doi.org/10.1016/j.radmeas.2015.02.001, 2015.

Mauz, B., Martin, L., Discher, M., Tribolo, C., Kreutzer, S., Bahl, C., Lang, A., and Mercier, N.: Technical note: On the reliability of laboratory beta-source calibration for luminescence dating, Geochronology, 3, 371–381, https://doi.org/10.5194/gchron-3-371-2021, 2021.

Murray, A.S. and Wintle, A.G.: Luminescence dating of quartz using an improved single-aliquot regenerative-dose protocol, Radiat. Meas., 32, 57–73, https://doi.org/10.1016/S1350-4487(99)00253-X, 2000.

Richter, D., Woda, C., and Dornich, K.: A new quartz for γ -transfer calibration of radiation sources, Geochronometria, 47, 23–34, https://doi.org/10.2478/geochr-2020-0020, 2020.

Sauer, D., Kadereit, A., Kühn, P., Kösel, M., Miller, C.E., Shinonaga, T., Kreutzer, S., Herrmann, L., Fleck, W., Starkovich, B.M., and Stahr, K.: The loess-palaeosol sequence of Datthausen, SW Germany: Characteristics, chronology, and implications for the use of the Lohne Soil as a marker soil, Catena, 146, 10–29, https://dx.doi.org/10.1016/j.catena.2016.06.024, 2016.

Thomsen, K.J., Murray, A.S., Jain, M., and Bøtter-Jensen, L.: Laboratory fading rates of various luminescence signals from feldspar-rich sediment extracts, Radiat. Meas., 43, 1474–1486, https://doi.org/10.1016/j.radmeas.2008.06.002, 2008.

Tribolo, C., Kreutzer, S., and Mercier, N.: How reliable are our beta-source calibrations?, Ancient TL, 37, 1–10, https://hal.archives-ouvertes.fr/hal-02165583, 2019.

Tudyka, K., Miłosz, S., Adamiec, G., Bluszcz, A., Poręba, G., Paszkowski, Ł., and Kolarczyk, A.: μDose: A compact system for environmental radioactivity and dose rate measurement, Radiat. Meas., 118, 8–13, https://doi.org/10.1016/j.radmeas.2018.07.016, 2018.

Tudyka, K., Bluszcz, A., Poręba, G., Miłosz, S., Adamiec, G., Kolarczyk, A., Kolb, T., Lomax, J., and Fuchs, M.: Increased dose rate precision in combined α and β counting in the μDose system - a probabilistic approach to data analysis, Radiat. Meas., 134, 106310, https://doi.org/10.1016/j.radmeas.2020.106310, 2020.

Wintle, A.G.: Anomalous fading of thermo-luminescence in mineral samples, Nature, 245, 143–144, https://www.nature.com/articles/245143a0, 1973.

Results – Luminescence Screening

Table S1: Analytical dose rate data and effective dose rates for the pIR$_{125}$BLSL$_{125}$-protocol.

Lab.-No./subsample/depth/horizon	DL_kosm	Err_DL_kosm	U	Err_U	Th	Err_Th	K	Err_K	Water_meas	Water_mod	Err_Water_mod	a_value.fine_grain	Err_a_value.fine_grain	K_grain_intern	Err_K_grain_intern	Grain_min	Grain_max	a_value	Err_a_value	DL_eff	Err_DL_eff
HDS-1802_C_672.5 cm_3BCk3	0.1044	0.0104	2.600	0.320	11.831	1.043	1.534	0.049	1.065	1.17	0.05	0.035	0.02	0	0	125	212	0.0295	0.0168	2.9168	0.2167
HDS-1804_B_764.5 cm_5Bw2	0.0957	0.0096	2.384	0.310	13.746	1.126	1.452	0.048	1.075	1.17	0.05	0.035	0.02	0	0	125	212	0.0295	0.0168	2.9258	0.2252
HDS-1808_E_963.5 cm_5Ck2	0.0801	0.0080	1.596	0.240	11.585	0.820	1.310	0.045	1.050	1.17	0.05	0.035	0.02	0	0	125	212	0.0295	0.0168	2.4345	0.1776
HDS-1811_F_1091.5 cm_6Bw3	0.0719	0.0072	2.741	0.320	11.762	1.110	1.409	0.047	1.046	1.17	0.05	0.035	0.02	0	0	125	212	0.0295	0.0168	2.8093	0.2189
HDS-1815_E_1256.5 cm_7Btg	0.0629	0.0063	2.072	0.220	13.207	0.750	1.482	0.046	1.086	1.17	0.05	0.035	0.02	0	0	125	212	0.0295	0.0168	2.8006	0.2053
HDS-1817_E_1349.5 cm_8Bt1	0.0586	0.0059	2.858	0.330	12.018	1.213	1.480	0.049	1.157	1.17	0.05	0.035	0.02	0	0	125	212	0.0295	0.0168	2.9039	0.2269
HDS-1817_E_1349.5 cm_8Bt1 - wetter	0.0586	0.0059	2.858	0.330	12.018	1.213	1.480	0.049	1.157	1.28	0.05	0.035	0.02	0	0	125	212	0.0295	0.0168	2.6165	0.1984

Table S2: Analytical dose rate data and effective dose rates for the pIR$_{60}$IR$_{225}$-protocol.

Lab.-No./subsample/depth/horizon	DL_kosm	Err_DL_kosm	U	Err_U	Th	Err_Th	K	Err_K	Water_meas	Water_mod	Err_Water_mod	a_value.fine_grain	Err_a_value.fine_grain	K_grain_intern	Err_K_grain_intern	Grain_min	Grain_max	a_value	Err_a_value	DL_eff	Err_DL_eff
HDS-1802_C_672.5 cm_3BCk3	0.1044	0.0104	2.600	0.320	11.831	1.043	1.534	0.049	1.065	1.17	0.05	0.1	0.02	12.5	1.25	125	212	0.0842	0.0168	4.1083	0.2307
HDS-1804_B_764.5 cm_5Bw2	0.0957	0.0096	2.384	0.310	13.746	1.126	1.452	0.048	1.075	1.17	0.05	0.1	0.02	12.5	1.25	125	212	0.0842	0.0168	4.1492	0.2396
HDS-1808_E_963.5 cm_5Ck2	0.0801	0.0080	1.596	0.240	11.585	0.820	1.310	0.045	1.050	1.17	0.05	0.1	0.02	12.5	1.25	125	212	0.0842	0.0168	3.5212	0.1882
HDS-1811_F_1091.5 cm_6Bw3	0.0719	0.0072	2.741	0.320	11.762	1.110	1.409	0.047	1.046	1.17	0.05	0.1	0.02	12.5	1.25	125	212	0.0842	0.0168	4.0126	0.2334
HDS-1815_E_1256.5 cm_7Btg	0.0629	0.0063	2.072	0.220	13.207	0.750	1.482	0.046	1.086	1.17	0.05	0.1	0.02	12.5	1.25	125	212	0.0842	0.0168	3.9786	0.2154
HDS-1817_E_1349.5 cm_8Bt1	0.0586	0.0059	2.858	0.330	12.018	1.213	1.480	0.049	1.157	1.17	0.05	0.1	0.02	12.5	1.25	125	212	0.0842	0.0168	4.1257	0.2424
HDS-1817_E_1349.5 cm_8Bt1 - wetter	0.0586	0.0059	2.858	0.330	12.018	1.213	1.480	0.049	1.157	1.28	0.05	0.1	0.02	12.5	1.25	125	212	0.0842	0.0168	3.7673	0.2111

HDS-1802 (flower box sample HDS-1802 F – G) – $BLSL_{125}$ – I 1 – 1 (0 – 0.16 s) – LL 201 – 250 (32.16 – 40 s)			
Subsample	**I 1 – 1 s, LL 151 – 200 s**	**I 1 – 1 s, LL 151 – 200 s**	**I 1 – 1 s, LL 151 – 200 s**
F **Aliquots 1 – 3** from left to right	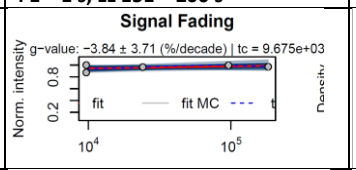	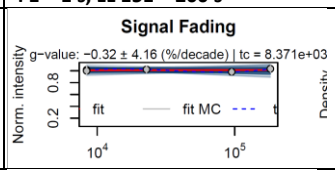	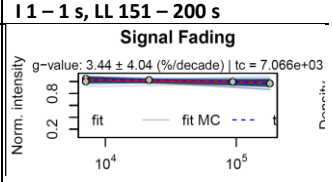
G **Aliquots 1 – 3** from left to right	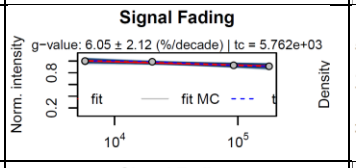	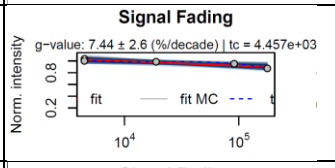	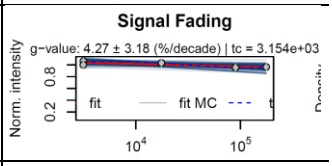
combine aliquots **F (aliquot 1 – 3)** **G (aliquots 1 – 3)** **F, G (all aliquots)** from left to right	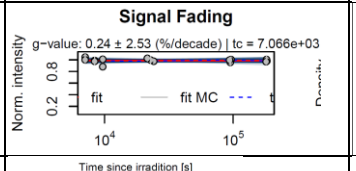	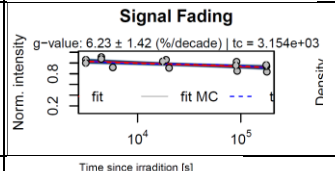	
	Time since irradition [s] $[\log_{10}(t/t_c)]$	Time since irradition [s] $[\log_{10}(t/t_c)]$	Time since irradition [s] $[\log_{10}(t/t_c)]$
g-value normalised to 2 days [%/decade]:	**F-1:** -3.66 ± 3.9 **F-2:** -0.32 ± 4.4 **F-3:** 3.61 ± 4.28 **G-1:** 6.65 ± 2.19 **G-2:** 8.44 ± 2.72 **G-3:** 4.61 ± 3.37 **F1 – F3:** 0.24 ± 2.63 **G-1 – G-3:** 6.99 ± 1.46		

HDS-1802 (box samples HDS-1802, subsample F (aliqout 1–3) and subsample G (aliquot 1–3) – $BLSL_{125}$ – including the three readouts. Delays: "prompt", ca 4 h, ca 1 day, ca 2 days "prompt".

Figure S1: Results of the *g*-value determination: $BLSL_{125}$ signal, box sample HDS-1802, subsamples F–G. While the three aliquots of subsample HDS-1802 F show within error margins *g*-values around zero (no fading), the three aliquots of subsample HDS-1802 G show g-values around ca 7.

HDS-1817 (flower box sample HDS-1817 A, B, C, D) – $BLSL_{125}$ – I 1 – 1 (0 – 0.16 s) – LL 201 – 250 (32.16 – 40 s)			
Subsample	**I 1 – 1 s, LL 151 – 200 s**	**I 1 – 1 s, LL 151 – 200 s**	**I 1 – 1 s, LL 151 – 200 s**
A **Aliquots 1 [1], 3 [3]** from left to right	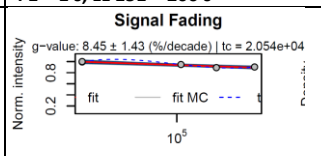		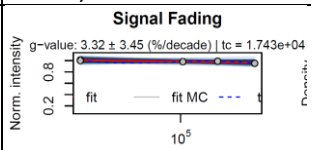
B **Aliquots 1 [4]** from left to right	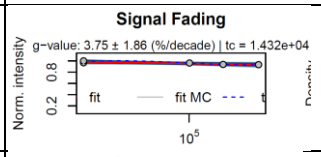		
C **Aliquots 1 [7], 3 [9]** from left to right	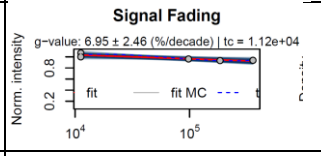		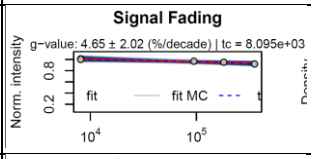
D **Aliquots 3 [12]** from left to right			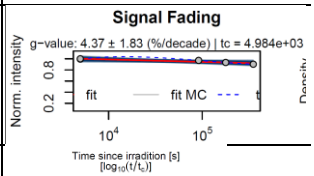
	Time since irradition [s] $[\log_{10}(t/t_c)]$	Time since irradition [s] $[\log_{10}(t/t_c)]$	Time since irradition [s] $[\log_{10}(t/t_c)]$
g-value normalised to 2 days [%/decade]:	**A-1 [1]:** 9.17 ± 1.44 **A-3 [3]:** 3.43 ± 3.57 **B-1 [4]:** 3.91 ± 1.9 **C-1 [7]:** 7.58 ± 2.53 **C-3 [9]:** 4.95 ± 2.07 **D-3 [12]:** 4.69 ± 1.88		

HDS-1817 (box sample HDS-1817, subsample A (1,3), subsample B (aliquot 1, turntable position 4), subsample C (aliquot 1,3, position 7,9) and subsample D (aliqout 3, position 12) – $BLSL_{125}$ – including the three prompt readouts. Delays: "prompt", ca 1 day, ca 2 days, ca 4 days "prompt".

Figure S2: Results of the *g*-value determination: $BLSL_{125}$ signal, box sample HDS-1817, subsamples A, B, C, D. While one aliquot of subsample HDS-1817 A shows a *g*-value which within the comparably large error margin does not differ from zero, the other aliquots show *g*-values between ca 4 and 9.

HDS-1803 (flower box sample HDS-1803 A - H) – IR_{225} – including the three prompt readouts

Subsample	I 1 – 4 s, LL 51 – 60 s	I 1 – 4 s, LL 51 – 60 s	I 1 – 4 s, LL 51 – 60 s	I 1 – 4 s, LL 51 – 60 s
A, B, C, D	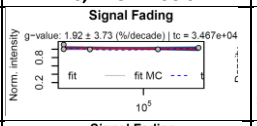	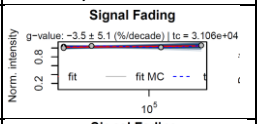	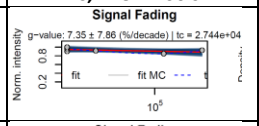	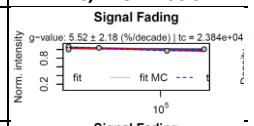
E, F, G, H	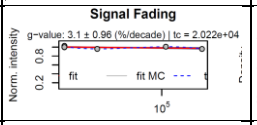	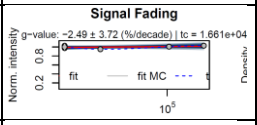	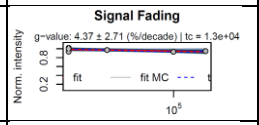	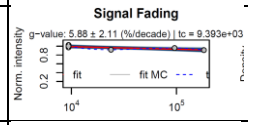
combine aliquots A - H	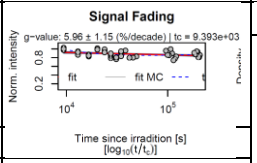	Time since irradition [s] [log10(t/tc)]	Time since irradition [s] [log10(t/tc)]	Time since irradition [s] [log10(t/tc)]
g-value normalised to 2 days [%/decade]:	**A:** 1.95 ± 3.83 **B:** -3.41 ± 5.3 **C:** 7.8 ± 8.39 **D:** 5.79 ± 2.22 **E:** 3.19 ± 0.97 **F:** -2.42 ± 3.86 **G:** 4.59 ± 2.79 **H:** 6.35 ± 2.17 **A – H:** 6.45 ± 1.16	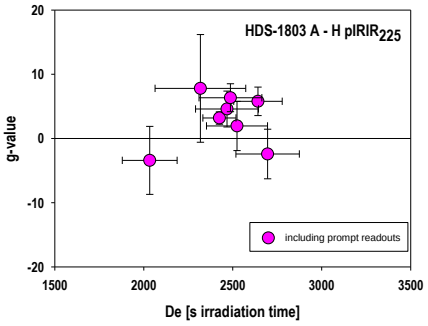		

HDS-1803 (flower box sample HDS-1803 A - H) – IR_{225} – including the three prompt readouts

(a)

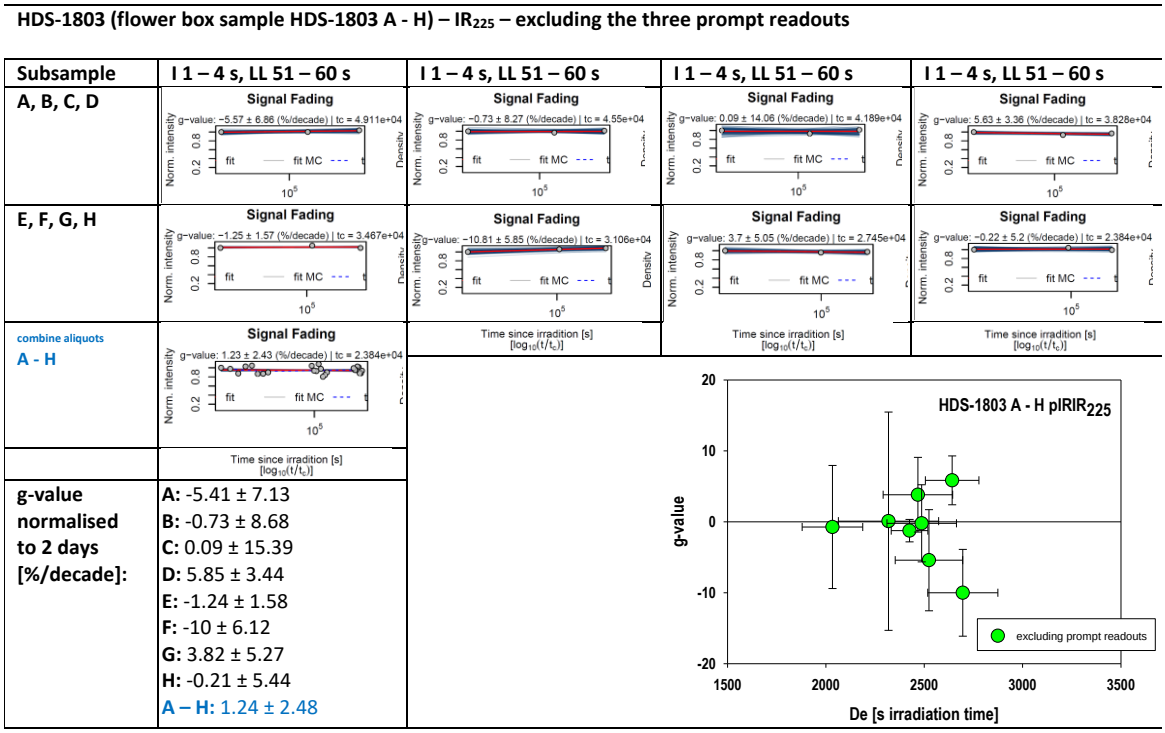

(b)

Figure S3: Results of the *g*-value determination: IR_{225} signal, box sample HDS-1803, subsamples A–H. (a) including the three prompt readouts, (b) excluding the three prompt readouts. Eliminating the prompt readouts leads to smaller *g*-values, mostly in agreement with zero-fading.

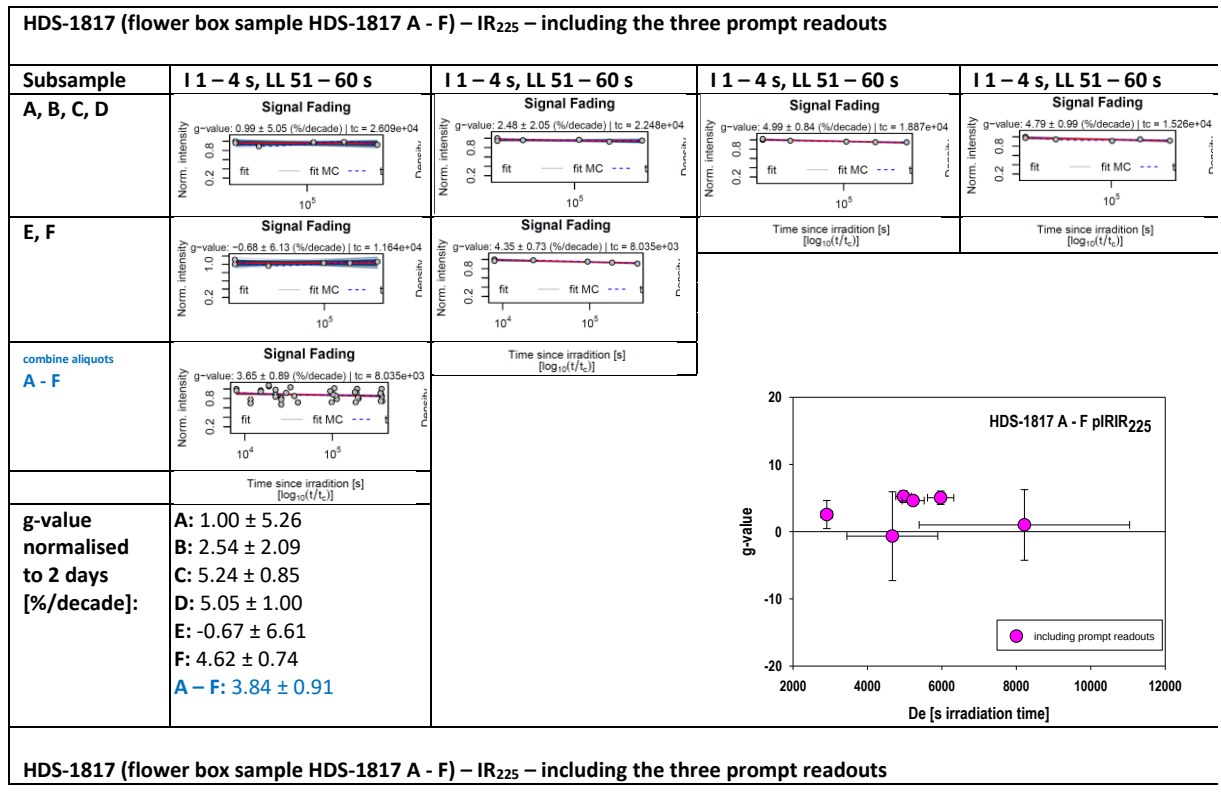

(a)

HDS-1817 (flower box sample HDS-1817 A - F) – IR_{225} – excluding three prompt readouts

Subsample	I 1 – 4 s, LL 51 – 60 s	I 1 – 4 s, LL 51 – 60 s	I 1 – 4 s, LL 51 – 60 s	I 1 – 4 s, LL 51 – 60 s
A, B, C, D	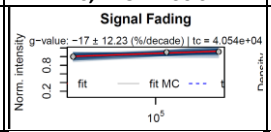	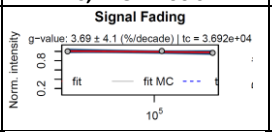	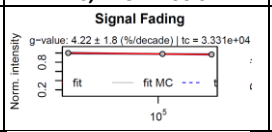	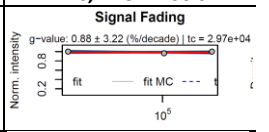
E, F	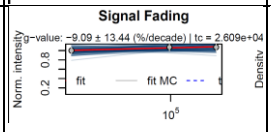	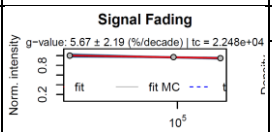	Time since irradition [s] [$\log_{10}(t/t_c)$]	Time since irradition [s] [$\log_{10}(t/t_c)$]
combine aliquots A - F	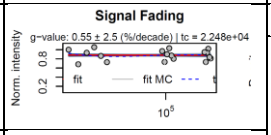	Time since irradition [s] [$\log_{10}(t/t_c)$]	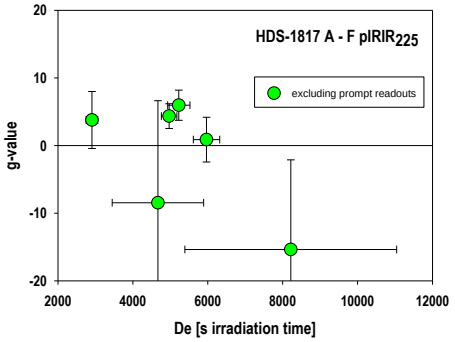	
	Time since irradition [s] [$\log_{10}(t/t_c)$]			
g-value normalised to 2 days [%/decade]:	**A:** -15.36 ± 13.25 **B:** 3.78 ± 4.21 **C:** 4.36 ± 1.83 **D:** 0.88 ± 3.31 **E:** -8.46 ± 15.1 **F:** 5.97 ± 2.23 **A – F:** 0.55 ± 2.56			

HDS-1817 (flower box sample HDS-1817 A - F) – IR_{225} – excluding the three prompt readouts

(b)

Figure S4: Results of the *g*-value determination: IR_{225} signal, box sample HDS-1817, subsamples A–F. (a) including the three prompt readouts, (b) excluding the three prompt readouts. Eliminating the prompt readouts leads to smaller *g*-values, mostly in agreement with zero-fading.

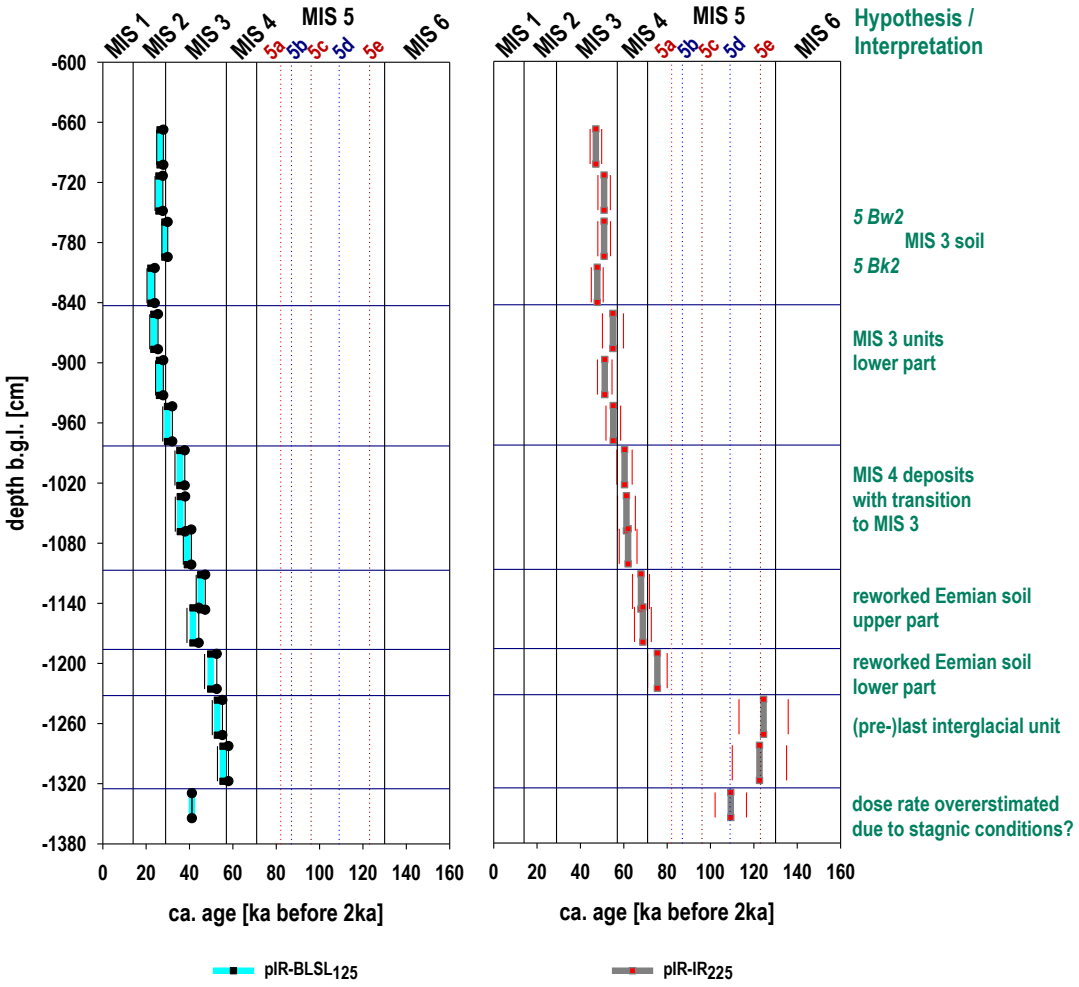

Figure S5: Results of the pIR-BLSL and $pIR_{60}IR_{225}$-screening summarised per box (HDS-1802 to HDS-1817, from top to bottom). Central "age estimates" (Galbraith et al., 1999) represented by broad light blue and grey bars, error ranges by thin black and red lines. D_eS determined with the software "Luminescence Analyst" (Duller, 2015). "Age estimate" assessments by assuming a representative effective dose rate of 2.80 Gy/ka for the pIR-BLSL protocol and 3.98 Gy/ka for the $pIR_{60}IR_{225}$ protocol. For details on the dose rate assessment cf. supplement 1 "Methods – Luminescence screening".

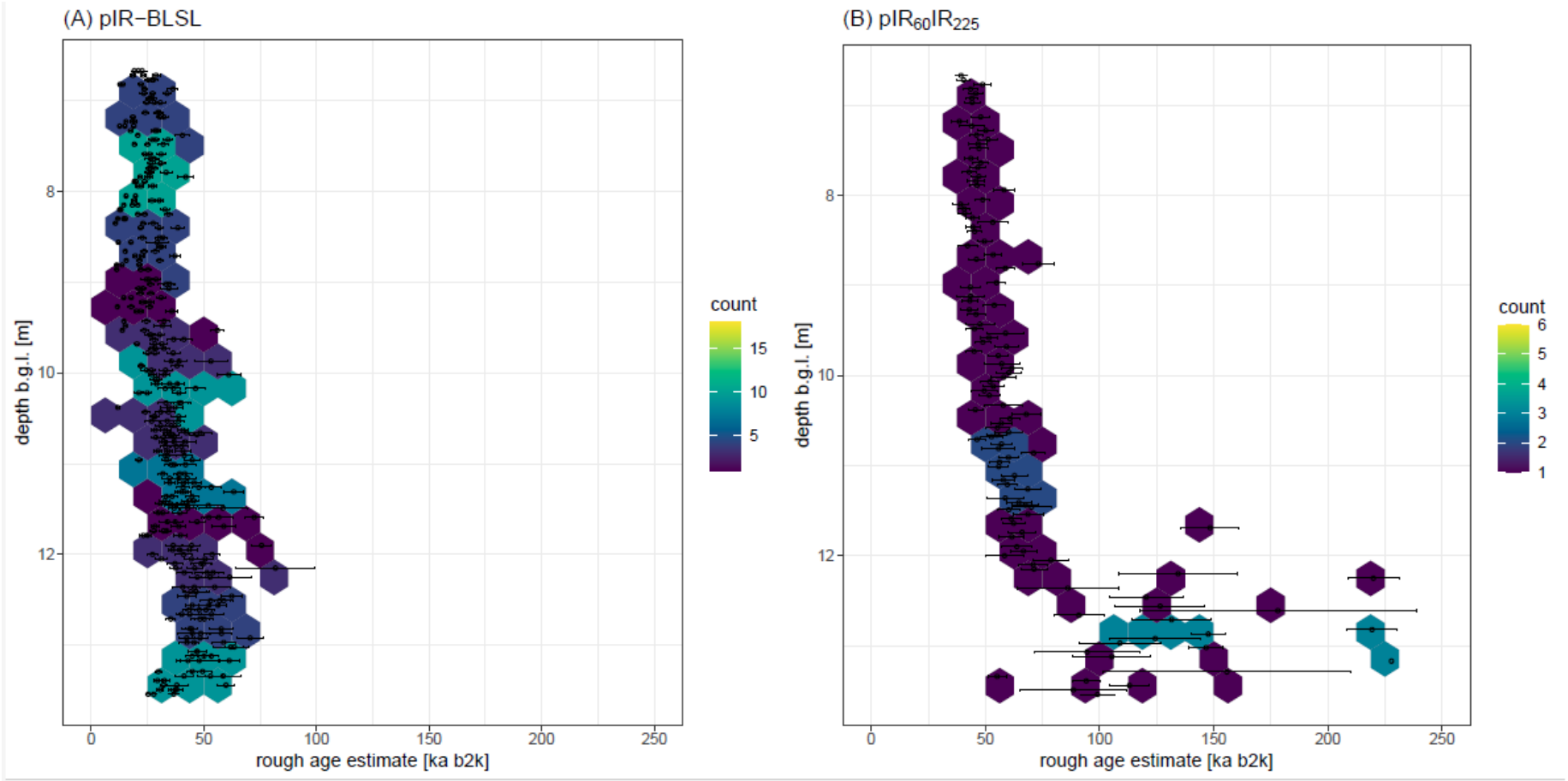

Figure S6: Representation of the age estimate-depth relationship of the results of the pIR-BLSL (A) and $pIR_{60}IR_{225}$-screening (B) as hexbinplot (also hexplot), in which the scattering of the data is reduced by binning (here maximum of 20 per hexagon). Counts equal the number of "age estimates" in one hexagon area. The figure shows the general pattern of the "age estimates", which generally increase with depth. The $pIR_{60}IR_{225}$ "age estimates" are systematically older than the pIR-BLSL-"age estimates".